ACS OMEGA

Open Access

http://pubs.acs.org/journal/acsodf

Article

Proteomics Analysis Provides Insights into the Role of Lipid Metabolism in T2DM-Related Sarcopenia

Jingying Wu, Shengnan Wang, Huafeng Zhuang, Weichun Wang, Yaoguo Wang, Youfang Chen, Zhengping Huang, Chunnuan Chen,* and Xiaofeng Chen*

Cite This: *ACS Omega* 2024, 9, 34056−34069

Read Online

ACCESS | Metrics & More | Article Recommendations | Supporting Information

ABSTRACT: Sarcopenia has been recognized as an emerging complication of type 2 diabetes mellitus (T2DM). Currently, the pathogenesis of T2DM-related sarcopenia remains unclear. The aim of this study was to investigate the molecular mechanisms and potential therapeutic targets for T2DM-related sarcopenia. In this study, a T2DM-related sarcopenia mouse model was established using db/db mice. Proteins extracted from the gastrocnemius muscles of db/db mice and littermate control db/m mice were analyzed by a 4D label-free quantitative proteomics approach. A total of 131 upregulated and 68 downregulated proteins were identified as differentially expressed proteins (DEPs). Bioinformatics analysis revealed that DEPs were significantly enriched in lipid metabolism. Protein−protein interaction network analysis revealed that six hub proteins, including ACOX1, CPT2, ECI2, ACADVL, ACADL, and ECH1, were involved in the fatty acid oxidation. The hub protein-transcription factor-miRNA network was also constructed using the NetworkAnalyst tool. Finally, the hub proteins were validated by Western blotting and immunohistochemistry and further confirmed to be significantly negatively correlated with muscle mass and grip strength. Our study suggested that lipid metabolism, especially excessive fatty acid oxidation, may be a crucial contributor to the progression of T2DM-related sarcopenia and a common cause of the inter-relationship between T2DM and sarcopenia. Targeting lipid metabolism may be a promising therapeutic strategy for T2DM-related sarcopenia.

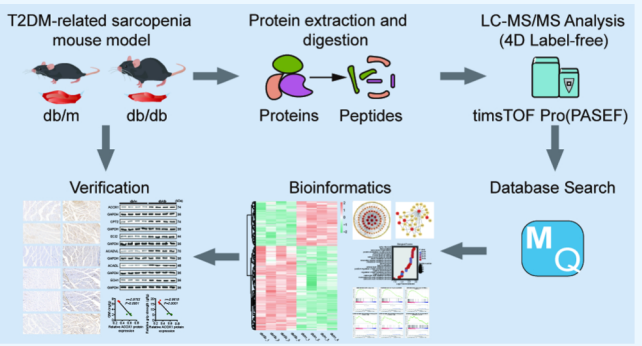

INTRODUCTION

Sarcopenia is a geriatric syndrome characterized by aging-related loss of skeletal muscle mass, strength, and function, leading to adverse outcomes such as frailty, disability, fractures, and even death in the elderly population.[1] While sarcopenia occurs primarily in older people, it can also occur secondary to chronic diseases, particularly diabetes mellitus, which is termed diabetes-related sarcopenia.[2,3] Type 2 diabetes mellitus (T2DM) is the most common metabolic disease in the world and manifests as an abnormal hyperglycemic state due to insulin resistance (IR) and insulin insufficiency.[4] T2DM is considered as a risk factor for numerous micro- and macrovascular complications, imposing a serious burden on public health.[5] Recently, sarcopenia is believed to be closely associated with T2DM.[6] IR can cause the deterioration of muscle mass and strength, while the loss of muscle mass in turn leads to decreased insulin sensitivity in skeletal muscle, resulting in a vicious cycle.[7] Studies have indicated that T2DM is associated with an accelerated decline in muscle mass and strength, with the rate of decline being positively correlated with both the duration of diabetes and elevated levels of HbA1c.[6,8] Likewise, the prevalence of sarcopenia is greater in the population with T2DM than in the nondiabetic population.[8,9] Sarcopenia has been recognized as an emerging complication of T2DM that not only detrimentally impacts diabetes progression and treatment response but also reduces muscle mass, strength, and physical performance, resulting in increased risk of physical disability, hospitalization, and mortality.[10] Diabetes-related sarcopenia has been a health concern worthy of close attention due to its detrimental impact on the quality of life and even survival. However, the pathogenesis of sarcopenia in individuals with T2DM and the common root cause of the inter-relationship between sarcopenia and T2DM remain elusive. Moreover, there is currently a lack of effective medical treatments for T2DM-related sarcopenia. In this context, a comprehensive understanding of the underlying molecular mechanisms of T2DM-related sarcopenia is urgently needed to explore potential therapeutic targets.

Received: May 16, 2024
Revised: July 7, 2024
Accepted: July 22, 2024
Published: July 26, 2024

Skeletal muscle serves as the primary tissue responsible for glucose disposal, accounting for up to 80% of insulin-stimulated glucose disposal.[11] Impaired insulin-stimulated glucose disposal in skeletal muscle, a condition known as IR, is considered a predominant contributor to the development of T2DM.[4,12] Given the role of skeletal muscle IR in diabetes, various "omics" analyses of skeletal muscles from diabetic animal models or patients with T2DM, including transcriptome,[13] proteome,[14] and metabolome[15] analyses, have been conducted to investigate the molecular mechanisms involved in the progression of T2DM. Nevertheless, these studies have largely focused on the mechanisms by which dysregulated metabolism in skeletal muscle contributes to diabetes, and the disease model of these studies involved diabetes alone without recognizing the comorbid occurrence of sarcopenia. There are a few studies of T2DM-related sarcopenia, and the role of T2DM in sarcopenia has received little attention. There is a complex bidirectional relationship between sarcopenia and T2DM. Sarcopenia has been confirmed to be both a cause and a consequence of T2DM.[10,11] Thus, it is equally important to study the mechanisms of T2DM-related sarcopenia as well as the potential common pathogenesis of T2DM and sarcopenia. Recently, proteomic analysis has been confirmed to be an advantageous approach for clarifying all proteins under both physiological and pathological conditions, as well as for identifying driver genes and potential targets for drug intervention.[16] To date, there is still a lack of proteomics studies focusing on T2DM-related sarcopenia.

In our study, we first employed db/db mice, a well-known mouse model of T2DM exhibiting the phenotype of extreme obesity. We further confirmed a mouse model of T2DM-related sarcopenia by assessing the muscle mass, grip strength, and histomorphological features of the skeletal muscle in db/db mice. Based on the successful construction of a mouse model of T2DM-related sarcopenia, a 4D label-free quantitative proteomics approach, characterized by its high sensitivity and accuracy in assessing abnormal protein expression, was performed on the gastrocnemius muscles (GMs) of db/db mice and littermate control db/m mice with normal blood glucose and body weight. Subsequently, bioinformatics analysis was utilized to explore the potential pathways and biological processes implicated in the progression of T2DM-related sarcopenia. Finally, Western blotting, immunohistochemistry, and correlation analysis were conducted to validate the candidate hub proteins of interest. The aim of the present study was to thoroughly elucidate the molecular mechanisms underlying sarcopenia in T2DM patients and to explore potential therapeutic targets for the treatment of T2DM-related sarcopenia.

MATERIALS AND METHODS

Antibodies. The primary antibodies used for immunoblotting and immunohistochemistry were as follows: anti-CPT2 antibody (26555-1-AP), anti-ACADVL antibody (14527-1-AP), anti-ACADL antibody (17526-1-AP), anti-ECH1 antibody (11385-1-AP), anti-ECI2 antibody (20383-1-AP), and anti-GAPDH antibody (60004-1-Ig) were obtained from Proteintech (Wuhan, China). Anti-ACOX1 antibodies (A21217) were obtained from ABclonal (Wuhan, China).

Animal Experiment and Tissue Collection. Eight-week-old male diabetic homozygous C57BLKS/J Iar-Leprdb/Leprdb mice (db/db mice) (n = 4) and eight-week-old male nondiabetic heterozygous C57BLKS/J Iar-m/leprdb mice (db/m mice) (n = 4) as the control were purchased from Shanghai SLACCAS Laboratory Animal Co., Ltd. (certificate of quality SCXK 2022−0004). All mice were housed in ventilated cages under SPF conditions with suitable humidity and temperature and kept on a 12-h light-dark cycle for 4 weeks. Standard laboratory chow and water were available ad libitum for mice. Body weight, fasting blood glucose, and grip strength were measured every week. All mice were fasted for 12 h overnight and sacrificed for collecting skeletal muscle samples at 12 weeks of age. GMs from the left and right sides were isolated and weighted quickly. The absolute mass of GM was determined based on the average mass of left and right GMs. Gastrocnemius muscle index (GMI) was defined as the absolute mass of GM divided by body weight to exclude the effect of body weight on muscle mass. Left GM tissues were divided into two parts. The proximal parts were fixed and stored in 4% paraformaldehyde for histological staining, whereas the distal parts were immediately frozen in liquid nitrogen and stored at −80 °C for Western blotting. Right GM tissues were also frozen in liquid nitrogen immediately and processed for a 4D label-free quantitative proteomics analysis. All experiments were approved by the Research Ethics Committee of the Second Affiliated Hospital of Fujian Medical University (Ethics Number: 2023-218).

Grip Strength Test. Grip strength was assessed using a mouse grip strength dynamometer (YLS13A, Nuoleixinda, Tianjin, China) to measure the grip strength of the four limbs of the mouse. A mouse was trained to grasp the horizontal grid attached to the dynamometer with four limbs and gently pulled backward in a horizontal direction parallel to the grid until the mouse released its grasp. Then the peak force applied to the grid was recorded. Each mouse was tested six times repeatedly for grip strength, and the six measured values were averaged as the absolute grip strength. The absolute grip strength was normalized to body weight to exclude the effect of body weight on muscle strength, which was defined as the relative grip strength.

Fasting Blood Glucose Test. Mice were fasted overnight for 12 h. Blood was obtained from the tail vein, and fasting blood glucose level was measured using a glucometer (Sinocare, Changsha, China) once per week.

Histological Analysis. Fixed GM tissues were dehydrated, paraffin-embedded, and sliced into 10-μm-thick sections. Hematoxylin and eosin (HE) staining and immunohistochemistry were performed after the paraffin sections were dewaxed and rehydrated. For morphological assessment and myofiber cross-sectional area (CSA) analysis, sections were stained with hematoxylin and eosin. Images were captured using a Nikon Eclipse E200 microscope (Nikon, Japan). Five randomly selected fields at 100× magnification were acquired from each section. The mean CSA of at least 250 fibers from five fields of each HE-stained section was analyzed by using ImageJ software. Immunohistochemistry stains were performed to evaluate the expression of CPT2, ACADVL, ACADL, ECH1, ECI2, and ACOX1. After antigen retrieval, sections were incubated in 3% hydrogen peroxide to quench the endogenous peroxidase and blocked with 10% bovine serum albumin. Then sections were incubated overnight at 4 °C with primary antibody (CPT2 rabbit polyclonal antibody, diluted 1:800; ACADVL rabbit polyclonal antibody, diluted 1:1000; ACADL rabbit polyclonal antibody, diluted 1:500, ECH1 rabbit polyclonal antibody, diluted 1:1000, ECI2 rabbit polyclonal

https://doi.org/10.1021/acsomega.4c04668
ACS Omega 2024, 9, 34056−34069

antibody, diluted 1:500; ACOX1 rabbit monoclonal antibody, diluted 1:1000). Subsequently, sections were incubated with secondary antibodies, developed with DAB and counterstained with hematoxylin. Photographs of stained sections were taken with a Nikon Eclipse E200 microscope (Nikon, Japan), and analyzed using Image-Pro Plus software.

Western Blot. Approximately 25 mg of tissues were dissected and homogenized in 500 μL of RIPA lysis buffer (Beyotime, Shanghai, China) with a Mill Cryogenic Grinder (KZ-III-FP, Servicebio Technology, Wuhan, China). Protein concentrations were detected by a BCA Protein Assay (Beyotime, Shanghai, China). Afterward, Western blot analysis was performed. Briefly, proteins were separated by sodium dodecyl sulfate polyacrylamide gel electrophoresis (10% and 12.5%) and blotted onto PVDF membranes. The PVDF membranes were blocked with 5% skimmed milk for 1 h at room temperature and incubated at 4 °C overnight with primary antibodies (anti-CPT2 antibody, anti-ACADVL antibody, anti-ACOX1 antibody, and anti-ECH1 antibody were diluted at 1:1000; anti-ACADL antibody and anti-ECI2 antibody were diluted at 1:500; anti-GAPDH antibody was diluted at 1:2000). Membranes were then washed with 1× tris-buffered saline with Tween and incubated with appropriate secondary antibodies. Finally, the membranes were developed using an ECL detection kit (Beyotime, Shanghai, China). Relative intensities of protein bands were quantified by using ImageJ software.

Protein Extraction. The frozen GM tissue was ground into cell powder with liquid nitrogen and then transferred to a 5 mL centrifuge tube. Afterward, four volumes of lysis buffer (8 M urea, 1% protease inhibitor cocktail) were added to the cell powder, followed by sonication three times on ice using a high-intensity ultrasonic processor (Scientz). The supernatant was collected after centrifugation (12,000*g*,10 min, 4 °C) and the remaining debris was removed. Finally, the protein concentration of each sample was determined with a BCA kit according to the manufacturer's instructions.

Trypsin Digestion. The protein solution was reduced with 5 mM dithiothreitol for 30 min at 56 °C and alkylated with 11 mM iodoacetamide for 15 min at room temperature in darkness. The protein sample was then diluted with 100 mM triethylammonium bicarbonate (TEAB) to a urea concentration less than 2 M. Next, trypsin was added at a 1:50 trypsin-to-protein mass ratio for the first digestion overnight and 1:100 trypsin-to-protein mass ratio for a second 4 h digestion. Finally, the peptides were desalted by a C18 SPE column.

Liquid Chromatography-Tandem Mass Spectrometry (LC-MS/MS) Analysis-4D Mass Spectrometry. The tryptic peptides were dissolved in solvent A (0.1% formic acid, 2% acetonitrile/in water) and directly loaded onto a homemade reversed-phase analytical column (25 cm length, 75/100 μm i.d.). Peptides were further separated using a nanoElute UHPLC system (Bruker Daltonics) at a constant flow rate of 450 nL/min with a gradient from 6 to 24% solvent B (0.1% formic acid in acetonitrile) over 70 min, 24 to 35% in 14 min, climbing to 80% in 3 min, then holding at 80% for the last 3 min. The separated peptides were subjected to a capillary source followed by timsTOF Pro (Bruker Daltonics) mass spectrometry. The electrospray voltage applied was 1.75 kV. The TOF detector was used to analyze precursors and fragments, with a MS/MS scan range from 100 to 1700 m/z. The timsTOF Pro was operated in the parallel accumulation serial fragmentation (PASEF) mode. Precursors with charge states of 0 to 5 were selected for fragmentation, and 10 PASEF-MS/MS scans were acquired per cycle. The dynamic exclusion was set to 30 s.

Database Search. The raw MS/MS data files were processed using the Maxquant search engine (v.1.6.15.0) against the Mus_musculus_10090_SP_20210721.fasta (17089 sequences) concatenated with the reverse decoy database for protein identification and quantification. Trypsin/P was specified as the cleavage enzyme, and up to two missing cleavages were allowed. Precursor ion mass tolerance was set as 20 ppm in the first search and 5 ppm in the main search, whereas fragment ion mass tolerance was set as 0.02 Da. Carbamidomethylation of Cys was specified as a fixed modification, protein N-terminal acetylation and oxidation of Met were specified as variable modifications. FDR was adjusted to <1%. Student's *t*-test was used to evaluate significant differences. The proteins with fold changes of >1.50 or <0.67 and *P*-values <0.05 were considered as differentially expressed proteins (DEPs).

Bioinformatics Analysis. The principal component analysis (PCA) was carried out using the FactoMineR package in the R programming language. The predicted proteins were annotated according to the Cluster of Orthologous Groups/Eukaryotic Orthologous Groups (COG/KOG) function classification with the EggNOG database (http://www.ncbi.nlm.nih.gov/COG/). Gene ontology (GO) annotation proteome was derived from the UniProt-GOA database (http://www.ebi.ac.uk/GOA/) and classified as three categories: biological process (BP), cellular component (CC), and molecular function (MF). Proteins that were not annotated by the UniProt-GOA database would be annotated by InterProScan software based on protein sequence alignment. KAAS, a Kyoto Encyclopedia of Genes and Genomes (KEGG) online service tool was used to annotate the protein's KEGG database description, followed by using KEGG mapper to match the corresponding pathways. The subcellular localization annotation was predicted using Wolfpsort software. The enrichment of protein domains was analyzed by using InterPro software. For GO, the KEGG pathway and protein domain functional enrichment analyses, a two-tailed Fisher's exact test was employed to identify the enrichment of DEPs against all identified proteins and *P*-values <0.05 were considered statistically significant. KEGG pathway analysis for DEPs was also performed using ClueGO (version 2.5.9, Cytoscape software, https://cytoscape.org/). Volcano plots of DEPs were generated using the "ggplot2" package in the R programming language. The heatmap plot was generated using the function heat maps.2 in R with the gplots package.

Protein−Protein Interaction (PPI) Network. The PPI network of DEPs was constructed using the Search Tool for the Retrieval of Interacting Genes/Proteins (STRING) database (version 12.0, https://string-db.org/) with a medium confidence score >0.4. The interaction network was then visualized using Cytoscape (version 3.9.1, https://cytoscape.org/). The molecular complex detection (MCODE) (version 2.0.2), a plugin of Cytoscape, was applied to identify highly interconnected subclusters of proteins based on the MCODE score and node number. Besides, CytoHubba plugin Cytoscape was applied to identify hub proteins. Subsequently, the network of miRNA associated with hub proteins was predicted using TarBase v8.0 in the NetworkAnalyst 3.0 tool (https://www.networkanalyst.ca/), whereas the transcription factor

https://doi.org/10.1021/acsomega.4c04668
ACS Omega 2024, 9, 34056−34069

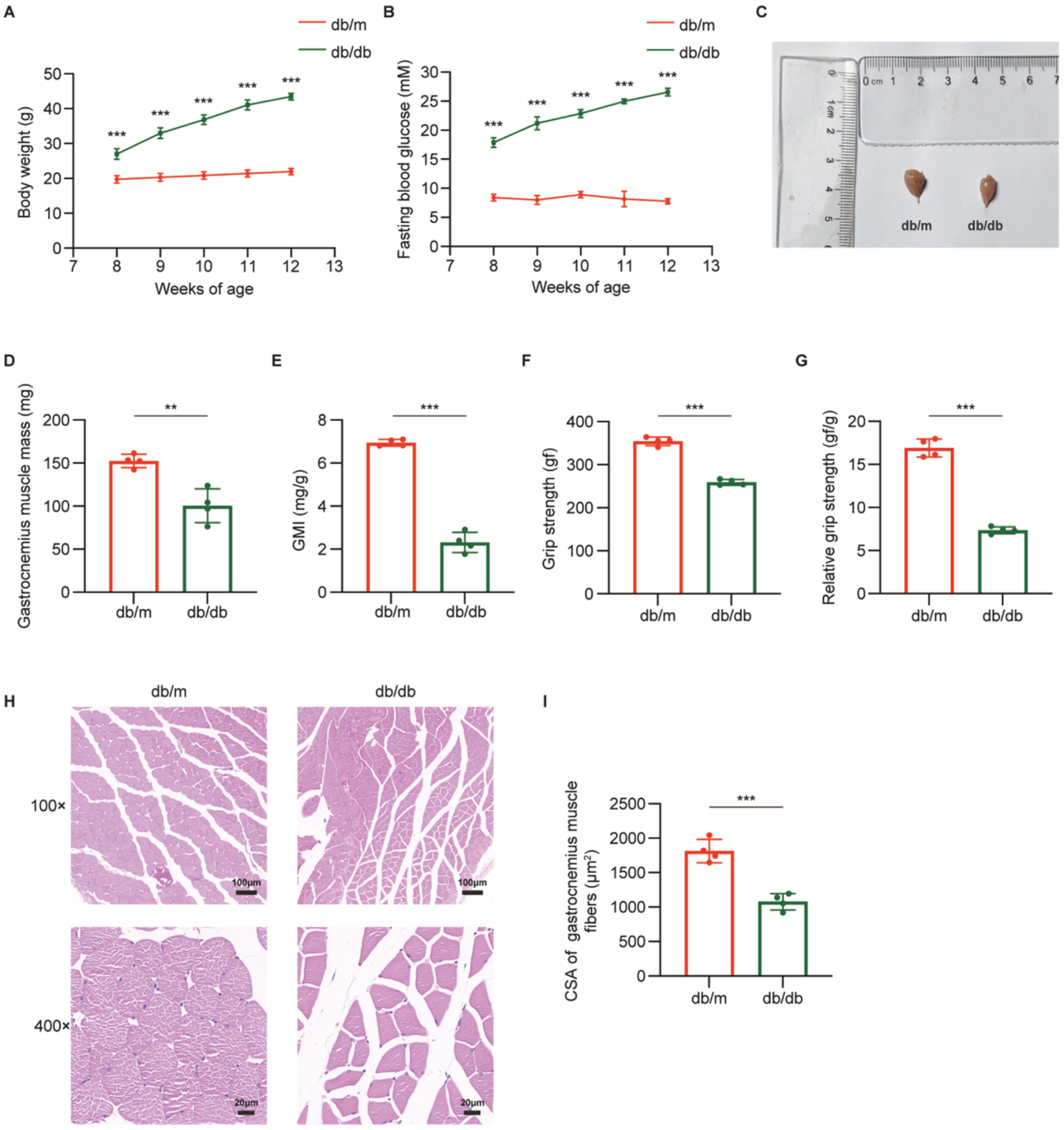

Figure 1. Establishment of an animal model of T2DM-related sarcopenia. (A) Comparison of the body weight curve between db/m mice and db/db mice. (B) Comparison of the fasting blood glucose curve between db/m mice and db/db mice. (C) Comparison of the GM morphology between db/m mice and db/db mice. (D−G) Comparison of gastrocnemius muscle mass, GMI, grip strength, and relative grip strength between db/m mice and db/db mice. (H−I) Comparison of HE staining and CSA of GM fibers between db/m mice and db/db mice. GMI, gastrocnemius muscle index. CSA, cross-sectional area. Scale bar: 20 and 100 μm. Data are expressed as mean ± SD $^{**}P < 0.01$, $^{***}P < 0.001$.

(TF)-hub protein network was also predicted using ENCODE in the NetworkAnalyst 3.0 tool. Both predicted networks of miRNA and TFs associated with hub proteins were visualized using Cytoscape.

Gene Set Enrichment Analysis (GSEA). The identified protein names were translated to gene names in R using the biomaRt package. GSEA was performed using the GSEA software (version 4.3.2) against C5 GO gene sets (GO biological process, GO cellular component, GO molecular function) downloaded from the molecular signature database (MSigDB). A gene set that satisfied normalized enrichment score (NES) > 1, *P*-value < 0.05, and false discovery rate (FDR) *q*-value < 0.2 was determined to be significant.

Statistical Analysis. Data are exhibited as the mean ± standard deviation (SD) and analyzed using Graph Prism 9.0 software. Comparisons between the db/m and db/db groups

https://doi.org/10.1021/acsomega.4c04668
ACS Omega 2024, 9, 34056−34069

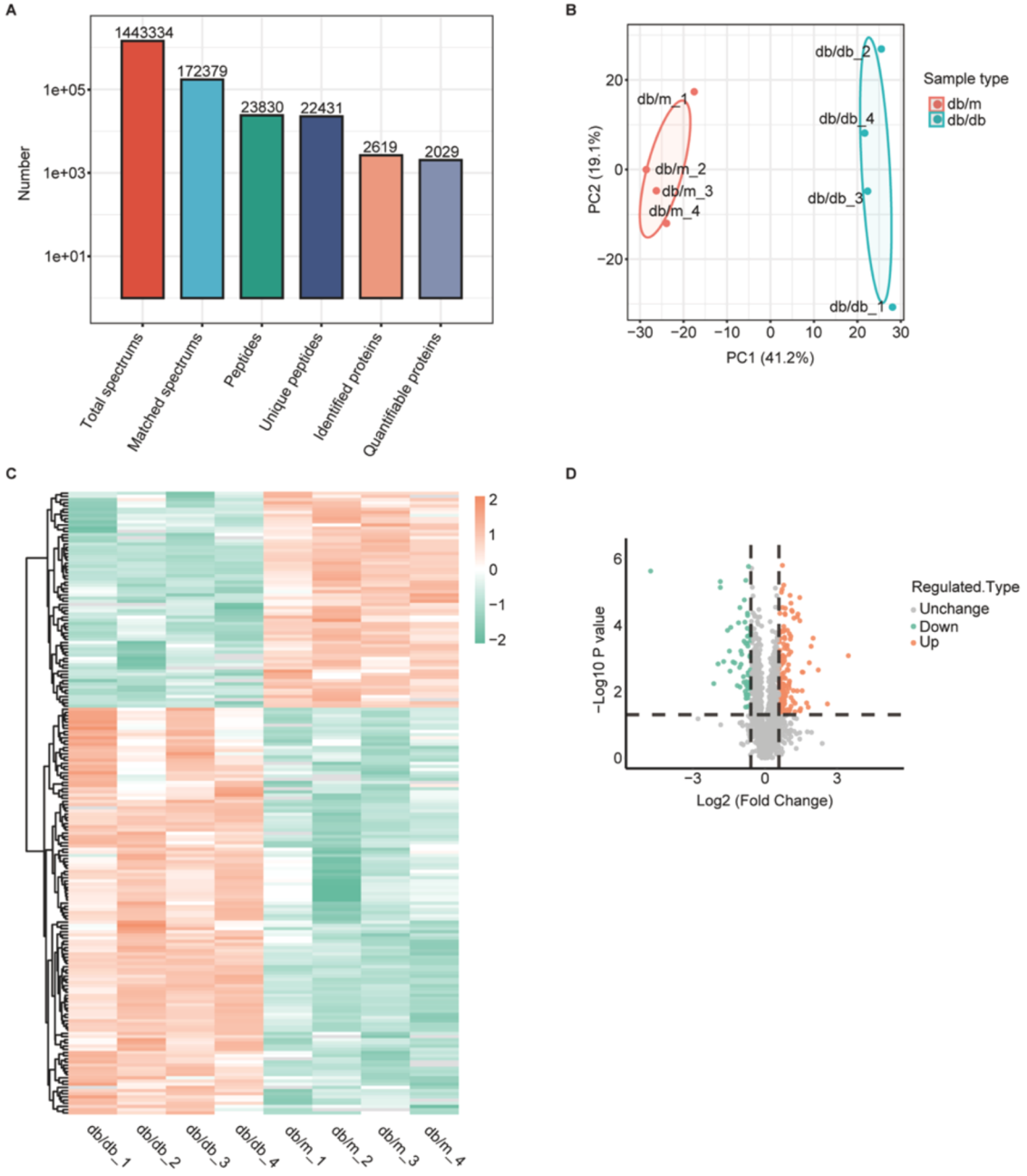

Figure 2. 4D label-free quantitative proteomics analysis of DEPs between db/db mice and db/m mice. (A) Results of database search analysis for mass spectrometry data. (B) PCA plot of proteome data. (C) Heatmap of DEPs between db/db mice and db/m mice. The orange color indicates upregulated proteins, while the green color indicates downregulated proteins. The color intensity indicates the degree of protein expression. (D) Volcano plot of DEPs. Orange dots indicate significantly upregulated proteins, green dots indicate significantly downregulated proteins, and gray dots represent proteins with no significant differences. PCA, principal component analysis. DEPs, differentially expressed proteins.

were performed using Student's *t*-test. Pearson correlation analysis was used for a simple linear correlation analysis. A value of $P < 0.05$ was considered statistically significant.

RESULTS

Establishment of an Animal Model of T2DM-Related Sarcopenia. The db/db mouse model is a well-known animal model of T2DM characterized by hyperglycemia, insulin resistance, and severe obesity.[17,18] As expected, both the body weight and fasting blood glucose of db/db mice aged 8 weeks to 12 weeks, were significantly greater than those of age-matched db/m mice (all $P < 0.05$). At 12 weeks of age, the db/db mice exhibited severe obesity and hyperglycemia, while the age-matched db/m mice exhibited steady weight gain and stable fasting blood glucose levels (Figure 1A,B). To confirm whether 12-week-old db/db diabetic mice could also exhibit a phenotype of sarcopenia, the muscle mass, grip strength, and histopathological characteristics of skeletal muscle were further measured. As shown in Figure 1C, the GM of db/db mice was smaller than that of db/m mice. Both the absolute mass of the GM and the GMI of the db/db mice were dramatically lower than those of the db/m mice (Figure 1D,E). Similarly, the muscle strength parameters, including the absolute and relative grip strength, of the db/db mice were also remarkably lower

https://doi.org/10.1021/acsomega.4c04668
ACS Omega 2024, 9, 34056−34069

Table 1. Top 10 Upregulated and Downregulated DEPs Identified from the db/db Mouse Group Compared to the db/m Mouse Group

protein accession	protein description	gene name	ratio	*P* value
	Upregulated			
Q99L88	β-1-syntrophin	Sntb1	11.098	0.000832
Q8R2Y2	cell surface glycoprotein MUC18	Mcam	6.072	0.023704
P24549	retinal dehydrogenase 1	Aldh1a1	4.657	0.002246
Q9R0H0	peroxisomal acyl-coenzyme A oxidase 1	Acox1	4.016	0.000247
P09541	myosin light chain 4	Myl4	3.793	0.000435
Q9D6M3	mitochondrial@2022 glutamate carrier 1	Slc25a22	3.599	0.001357
Q9WVC3	caveolin-2	Cav2	3.488	0.029633
P16110	galectin-3	Lgals3	3.331	0.022076
Q8K4G5	actin-binding LIM protein 1	Ablim1	2.989	0.00262
O35678	monoglyceride lipase	Mgll	2.932	0.00259
	Downregulated			
Q8BK84	dual specificity phosphatase 29	Dusp29	0.037	2.330×10^{-06}
P08074	carbonyl reductase [NADPH] 2	Cbr2	0.229	0.005773
Q9R112	sulfide quinone oxidoreductase	Sqor	0.259	0.001469
Q61699	heat shock protein 105 kDa	Hsph1	0.276	7.288×10^{-06}
Q921R8	solute carrier family 41-member 3	Slc41a3	0.276	4.845×10^{-06}
Q8BGM7	5′-AMP-activated protein kinase subunit γ-3	Prkag3	0.304	0.001249
Q9CR16	peptidyl-prolyl cis−trans isomerase D	Ppid	0.34	0.000143
P70266	6-phosphofructo-2-kinase/fructose-2,6-bisphosphatase 1	Pfkfb1	0.359	0.000605
Q8BLU2	protein-lysine methyltransferase METTL21C	Mettl21c	0.366	0.002427
Q9DBG1	sterol 26-hydroxylase, mitochondrial	Cyp27a1	0.373	0.000117

than those of the db/m mice (Figure 1F,G). In addition, HE staining revealed atrophic muscle fibers with irregular arrangement and widening of interstitial spaces in db/db mice, whereas muscle fibers in db/m mice were regularly and closely arranged (Figure 1H). The CSA of muscle fibers was significantly lower in db/db mice than in db/m mice (Figure 1I). All of the above data demonstrated the successful establishment of an animal model of T2DM-related sarcopenia.

Overview of 4D Label-Free Quantitative Proteomics Data and Identification of DEPs between db/db Mice and db/m Mice. The GMs collected from the db/db mice and db/m mice were subjected to LC-MS/MS analysis using a 4D label-free approach to obtain proteome profiles. Following strict quality control, a total of 1,443,334 spectra (172,379 matched) were obtained, and 23,830 peptides (22,431 unique peptides) were detected by spectral analysis. Based on the specific peptide segments, 2,029 proteins were quantified from a total of 2,619 identified proteins (Figure 2A). To ensure the quality of the proteomic data, the raw MS/MS data files were processed for a series of quality control evaluations after the database search. The lengths of most peptides ranged from 7 to 20 amino acids, suggesting that the samples met the quality control standards (Figure S1A). The molecular weight distribution of the identified proteins covered different sizes of proteins (Figure S1B). The coverage of most identified proteins ranged from 1 to 30% (Figure S1C). Most proteins were quantified by more than two peptides, indicating high reliability of the quantitative results (Figure S1D). Additionally, PCA revealed a significant difference between db/db mice and db/m mice (Figure 2B). Overall, these results supported the reliability and reproducibility of the MS proteomics data files.

Based on the statistical analysis, a total of 199 proteins with a fold-change of >1.50 or <0.67 and a *P* value less than 0.05 were identified as DEPs. Among these DEPs, 131 were upregulated, while 68 were downregulated. Furthermore, the heatmap depicted a hierarchical clustering of the DEPs (Figure 2C), while the volcano plot illustrated the average alterations in protein abundance for each individual protein (Figure 2D). The top 10 up- and downregulated DEPs are listed in Table 1.

Functional Annotation of DEPs. Subcellular structure analysis revealed that most of the DEPs were localized in the cytoplasm (38.19%), followed by the nucleus (16.58%), mitochondria (15.58%), extracellular space (14.07%), plasma membrane (8.54%), and both the cytoplasm and nucleus (4.02%). In addition to the subcellular locations described above, a fraction of the DEPs exhibited localization in other subcellular locations (3.02%) (Figure S2A). Subsequently, functional annotation via GO analysis was performed. The DEPs were classified into three categories, namely, BP, CC, and MF. According to the level 2 GO terms, the BP category was annotated into 11 subcategories, of which "cellular process", "biological regulation", "metabolic process", "response to stimulus", and "localization" were the top five GO terms; the CC category was annotated into 3 subcategories, including "cell", "intracellular", and "protein-containing complex"; and the MF category was annotated into 6 subcategories, of which "binding", "catalytic activity", "molecular function regulator", "structural molecule activity", and "transporter activity" were the top five GO terms (Figure S2B). Furthermore, the functional classification of DEPs was also determined using a COG/KOG analysis. The results demonstrated that the most abundant category was "signal transduction mechanisms" (27 proteins), followed by "lipid transport and metabolism" (22 proteins), "cytoskeleton" (21 proteins), "posttranslational modification, protein turnover, chaperones" (18 proteins) (Figure S2C).

Functional Enrichment Analysis of DEPs. To further investigate the potential biological functions and implications of the DEPs, functional enrichment analysis, including GO, KEGG pathway, and protein domain analyses were performed. Fisher's exact *t*-test with a filtering threshold of $P < 0.05$ was

https://doi.org/10.1021/acsomega.4c04668
ACS Omega 2024, 9, 34056−34069

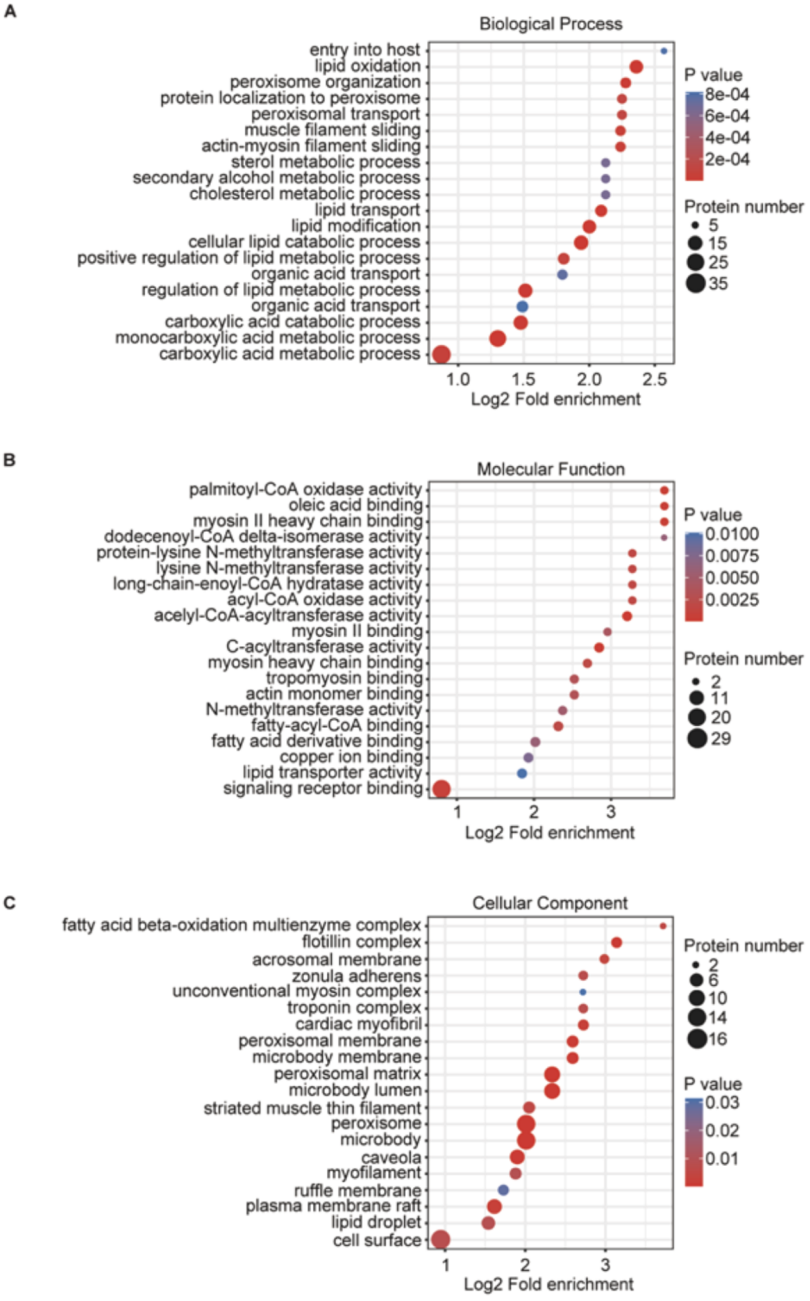

Figure 3. GO functional enrichment analysis of the DEPs. The DEPs were enriched into biological process (A), molecular function (B), and cellular component (C). The color key accompanying the bubble plot represents the significant *P* value for enrichment, while the size of the bubbles represents the number of DEPs in the respective functional class or pathway.

utilized to determine the significant functional enrichment levels of DEPs. As shown in Figure 3, the top 20 GO terms for enrichment classification are visualized in a bubble plot. The five most significant terms in the BP category were "lipid oxidation", "peroxisome organization", "protein localization to peroxisome", "peroxisomal transport", and "muscle filament sliding" (Figure 3A). The five most significant terms in the MF category were "palmitoyl-CoA oxidase activity", "oleic acid binding", "myosin II heavy chain binding", "long-chain-enoyl-CoA hydratase activity", and "lysine *N*-methyltransferase activity" (Figure 3B). The top five significant GO terms in the CC category were "flotillin complex", "microbody membrane", "peroxisomal membrane", "peroxisomal matrix", and "microbody lumen" (Figure 3C). Next, the DEPs were mapped to the KEGG database (Figure 4A) and ClueGO plugin of Cytoscape (Figure 4B) to explore enriched pathways. The top 10 significant pathways included "primary bile acid biosynthesis", "biosynthesis of unsaturated fatty acids", "α-linolenic acid metabolism", "PPAR signaling pathway", "fatty acid degradation", "sulfur metabolism", "peroxisome", "fatty acid elongation", "fat digestion and absorption", and "prostate cancer". The detailed information about the top 10 KEGG pathways is shown in Table S1. Additionally, the KEGG pathway analysis revealed that the upregulated DEPs were mainly enriched in metabolic pathways, and the top 5 significant pathways included "peroxisome", "PPAR signaling pathway", "fatty acid degradation", "biosynthesis of unsaturated fatty acids", and "Cardiac muscle contraction" (Table S2). On

https://doi.org/10.1021/acsomega.4c04668
ACS Omega 2024, 9, 34056−34069

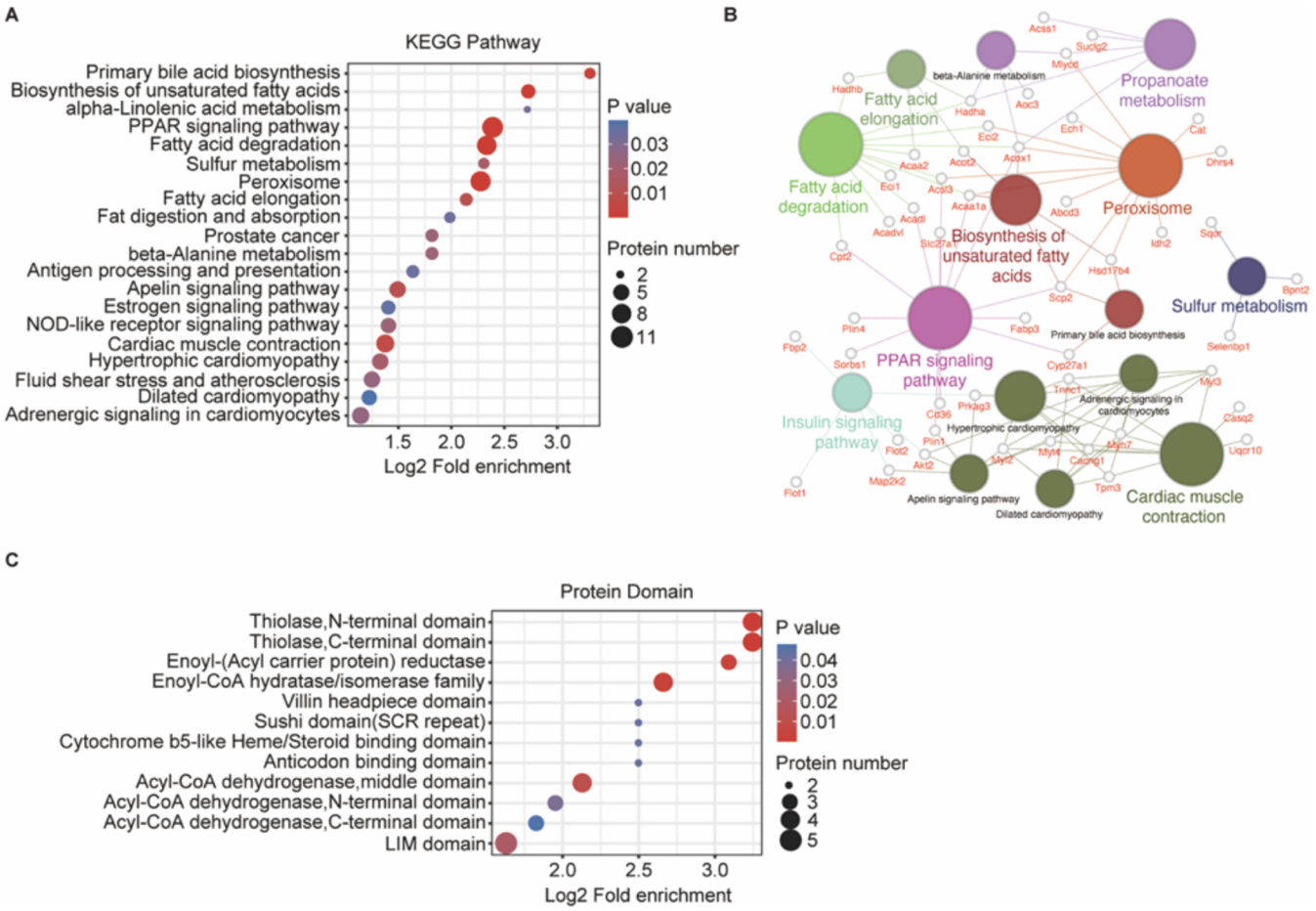

Figure 4. Functional enrichment analysis of KEGG and the protein domain for DEPs. (A) KEGG pathway enrichment analysis of DEPs. (B) Pathway enrichment analysis of DEPs using ClueGO in Cytoscape. (C) Protein domain enrichment analysis of DEPs.

the other hand, the KEGG pathway analysis of downregulated DEPs indicated that several functional pathways were enriched, and the top 5 significant pathways included "estrogen signaling pathway", "prostate cancer", "chemical carcinogenesis-receptor activation", "FoxO signaling pathway", and "Progesterone-mediated oocyte maturation" (Table S3). Taken together, these results suggested that significant changes in pathways, especially lipid metabolism-related pathways, may play a role in the onset of diabetes-induced sarcopenia. In addition, DEPs were subjected to protein domain analysis to investigate the domain functions of the DEPs. The results demonstrated that the DEPs mainly consisted of "thiolase, C-terminal domain", "thiolase, N-terminal domain", "enoyl-(acyl carrier protein) reductase", "enoyl-CoA hydratase/isomerase family", and "villin headpiece domain" (Figure 4C).

GSEA. GSEA is characterized by a wide range of enrichment analyses and serves to uncover potential disease mechanisms. Thus, we also utilized GSEA analysis to explore the functional enrichment of the identified proteins in greater depth. GSEA was carried out using the C5 GO gene sets in MSigDB. The results showed that the GO terms of the identified proteins were significantly enriched in "lipid oxidation", "fatty acid oxidation", "fatty acid catabolic process", "establishment of protein localization to peroxisome", "peroxisome organization", and "protein targeting to peroxisome", which were all ranked highly based on the normalized enrichment score (NES) (Figure 5A–F).

Construction of the PPI Network and the Hub Protein–TF–miRNA Network. To clarify the functional interactions of DEPs, a PPI network comprising 153 nodes and 600 edges was constructed using the STRING database and visualized with Cytoscape (Figure 6A). Next, the significant cluster with the highest score of 16.89 was determined using the MCODE plugin Cytoscape, which contained 19 nodes and 152 edges (Figure 6B). Then, CytoHubba plugin Cytoscape was used to identify the hub proteins. The six hub proteins, including acyl-coenzyme A oxidase 1(ACOX1), carnitine O-palmitoyltransferase 2(CPT2), enoyl-CoA delta isomerase 2 (ECI2), very long-chain specific acyl-CoA dehydrogenase (ACADVL), long-chain specific acyl-CoA dehydrogenase (ACADL), and delta (3,5)-delta (2,4)-dienoyl-CoA isomerase (ECH1), were obtained by intersecting the proteins obtained via the MCC, MNC, and degree methods (Table 2). Furthermore, the NetworkAnalyst online tool was used to predict the upstream TFs and miRNAs of the six hub proteins. The TF–hub protein network consisted of 31 nodes and 45 edges, of which five TFs, namely, GATA Binding Protein 1(GATA1), REST Corepressor 1(RCOR1), MYC Associated Zinc Finger Protein (MAZ), TATA-Box Binding Protein (TBP), and Nuclear Respiratory Factor 1(NRF1) were the common TFs of at least three hub proteins (Figure 6C). The miRNA-hub protein network contained 77 nodes and 93 edges. The mmu-mir-155–5p was found to be the common miRNA of ACOX1, CPT2, ECH1, ACADL, and ACADVL,

https://doi.org/10.1021/acsomega.4c04668
ACS Omega 2024, 9, 34056–34069

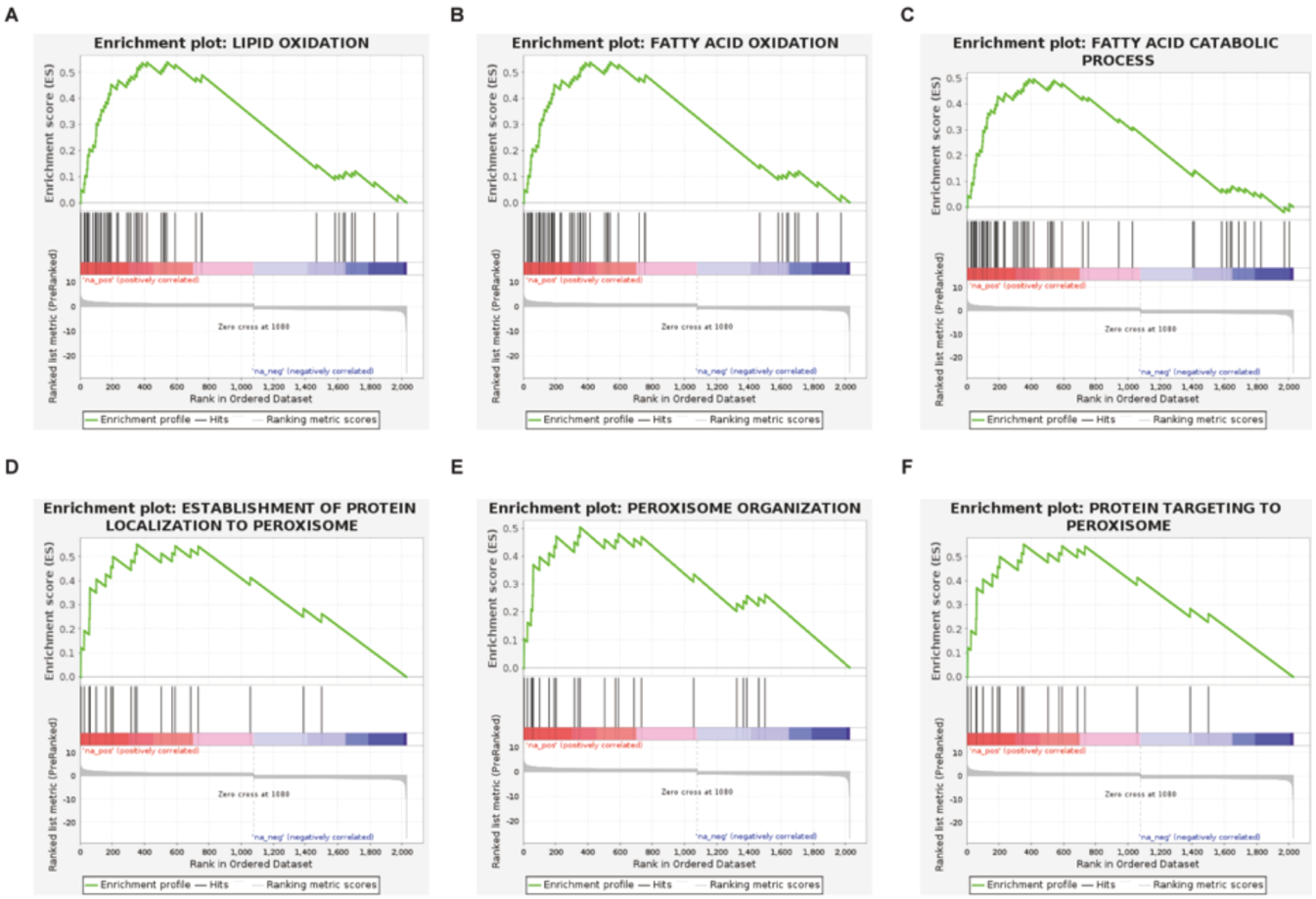

Figure 5. Results of the GSEA. (A) Enrichment plot of "lipid oxidation" with NES 3.42, FDR *q*-value 0.0. (B) Enrichment plot of "fatty acid oxidation" with NES 3.39, FDR *q*-value 0.0. (C) Enrichment plot of 'fatty acid catabolic process' with NES 3.32, FDR *q*-value 0.0. (D) Enrichment plot of "establishment of protein localization to peroxisome" with NES 2.54, FDR *q*-value 0.0. (E) Enrichment plot of "peroxisome organization" with NES 2.38, FDR *q*-value 0.01. (F) Enrichment plot of 'protein targeting to peroxisome' with NES 2.42, FDR *q*-value 0.01.

whereas mmu-mir-1a-3p was the common miRNA of CPT2, ECH1, and ACADL (Figure 6D).

Validation of Hub Protein Expression in Mice with T2DM-Related Sarcopenia. To confirm the proteomic analysis results, six hub proteins, ACOX1, CPT2, ECI2, ACADVL, ACADL, and ECH1, were validated by Western blotting and immunohistochemical staining. Both Western blotting and immunohistochemical staining revealed significantly greater expression of the six hub proteins in the GM of db/db mice than in that of db/m mice (Figure 7A–D). Moreover, correlation analysis revealed that the relative expression levels of the six hub proteins were negatively correlated to the relative grip strength and GMI (Figure 7E). The data above indicated that the six hub proteins may be involved in a diabetes-related decrease in skeletal muscle mass and strength.

DISCUSSION

A great deal of evidence suggests that a bidirectional association between sarcopenia and T2DM contributes to a vicious cycle of mutual aggravation, ultimately resulting in poor quality of life and serious health outcomes.[19−21] T2DM is an important etiological factor for the development of sarcopenia, as evidenced by various studies that have demonstrated a notable prevalence of sarcopenia in individuals with T2DM.[22] In contrast, the degeneration of skeletal muscle in sarcopenia patients deteriorates glucose metabolism and further increases the risk of T2DM development.[4] Since the significance of skeletal muscle in insulin-stimulated glucose disposal, previous studies have focused on the contributory role of skeletal muscle in T2DM, while the impact of T2DM on sarcopenia and the underlying mechanisms of the inter-relationship between diabetes and sarcopenia have received attention until recently. Given this background, we conducted a 4D label-free quantitative proteomics approach on skeletal muscles from db/db mice with sarcopenia, aiming to explore the potential mechanism of sarcopenia in T2DM and the contributors to the inter-relationship between T2DM and sarcopenia. In our study, we utilized a severe obesity and diabetes db/db mouse model, in which the manifestation of sarcopenia was confirmed. Since the atrophy of type II fibers, such as GM, appears to be more prevalent in T2DM-related sarcopenia,[13] proteomics analysis was performed on the GM from db/db mice and littermate control db/m mice. Our study showed that the identified DEPs were significantly enriched in metabolic pathways, particularly pathways linked to lipid metabolism. GSEA indicated that the fatty acid oxidation pathway may play a key role in the progression of T2DM-related sarcopenia. We also explored six hub proteins, namely, ACOX1, CPT2, ECI2, ACADVL, ACADL, and ECH1, which are involved in the fatty acid oxidation pathway. The hub protein−TF−miRNA network was further constructed to

https://doi.org/10.1021/acsomega.4c04668
ACS Omega 2024, 9, 34056−34069

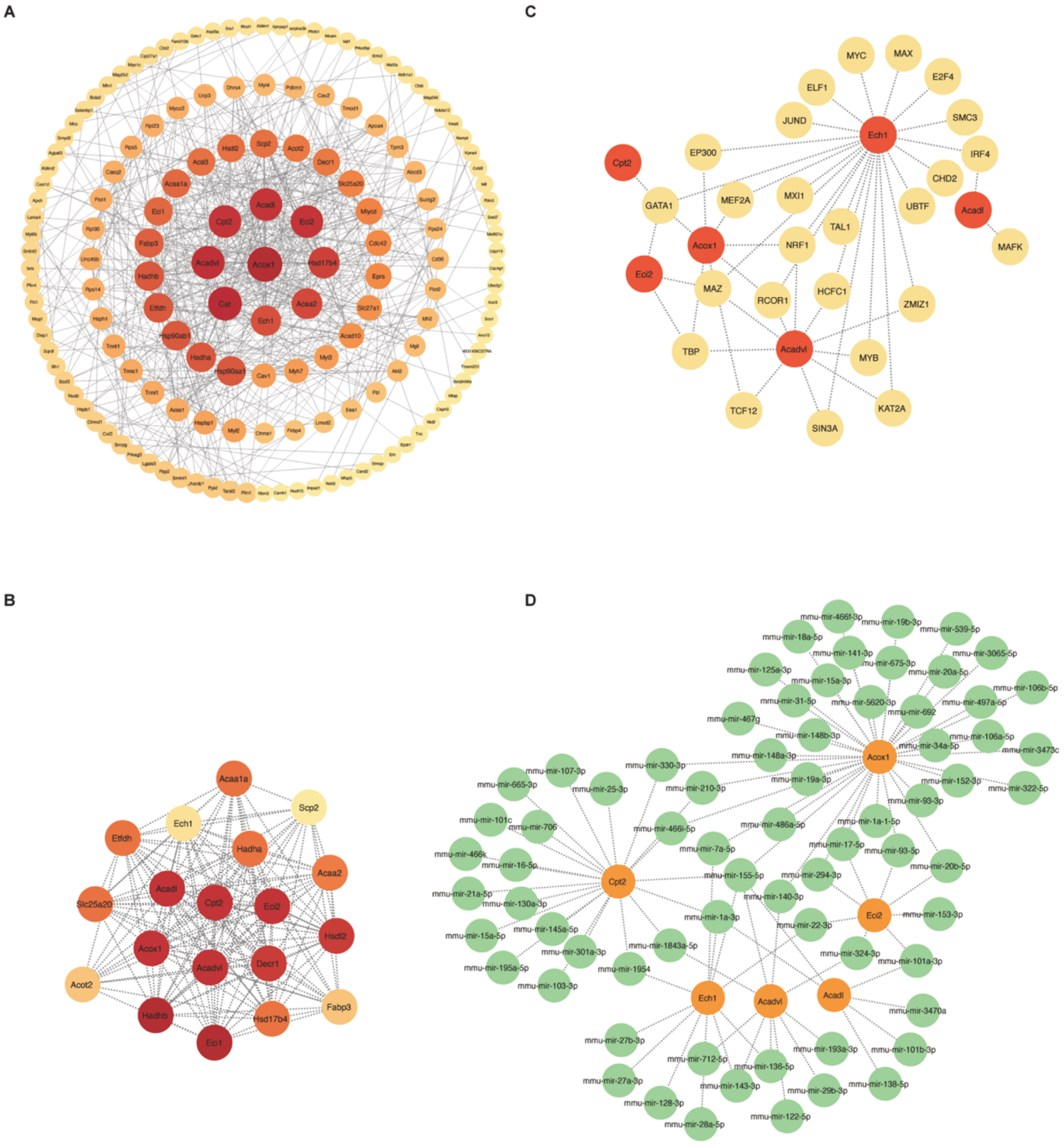

Figure 6. Construction of the PPI network and the hub protein−TF−miRNA network. (A) PPI network of DEPs. (B) Key cluster of DEPs explored by MCODE in Cytoscape. (C) TF−hub protein network: the red dots represent hub proteins, while the yellow dots represent TFs. (D) miRNA−hub protein network: the orange dots represent hub proteins and the green dots represent miRNAs.

better understand the underlying upstream regulators of the hub proteins. Finally, the six hub proteins were validated by Western blotting and immunohistochemistry. The hub proteins were also confirmed to be closely related to the low muscle mass and grip strength, indicating their contribution to T2DM-related sarcopenia.

Based on the functional enrichment analysis of DEPs, we found that the significant GO terms and KEGG pathways were both closely related to lipid metabolism. Skeletal muscle, a highly abundant tissue in the body, not only fulfills the crucial function of body movement but also plays a central role in whole-body metabolism.[23] In addition to being a major site of insulin-stimulated glucose disposal, skeletal muscle is also involved in whole-body lipid metabolism. Lipid metabolism is an important energy source for skeletal muscle fibers, since approximately two-thirds of resting skeletal muscle energy is derived from lipid oxidation.[24] Normally, skeletal muscle is not physiologically capable of storing lipids.[25] However, fat

https://doi.org/10.1021/acsomega.4c04668
ACS Omega 2024, 9, 34056−34069

Table 2. Top Six Hub Proteins Obtained by Three Algorithms of CytoHubba

MCC	MNC	Degree	Hub proteins
ACOX1	ACOX1	ACOX1	ACOX1
CPT2	ACADL	CAT	CPT2
ECI2	ACADVL	ACADVL	ECI2
ACADVL	CPT2	ACADL	ACADVL
ACADL	ECI2	ECI2	ACADL
ECH1	HSDL7B4	CPT2	ECH1
HADHA	ACAA2	HSDL7B4	
ETFDH	ECH1	ACAA2	
DECR1	HADHA	ECH1	

accumulation in skeletal muscle due to alterations in lipid metabolism, defined as myosteatosis, is evident in sarcopenia patients with aging and T2DM.[24] Myosteatosis has been recognized as one of the hallmarks of both primary and secondary sarcopenia.[26] Studies have revealed that myosteatosis provides a lipotoxic environment with mitochondrial dysfunction, increased reactive oxygen species (ROS) production, and enhanced secretion of proinflammatory myokines, leading to reduced muscle mass and strength.[27] On the other hand, aberrant lipid metabolism is known to be strongly associated with T2DM. Elevated circulating free fatty acids (FFAs) are common in individuals with T2DM, while myosteatosis has been identified as a key contributor to the onset of insulin resistance and T2DM.[28] Myosteatosis significantly influences glucose homeostasis in skeletal muscle by modulating insulin-stimulated glucose uptake, activating inflammatory signals, inducing endoplasmic reticulum stress, and causing mitochondrial dysfunction,[29] ultimately contributing to the progression of T2DM. Overall, aberrant lipid metabolism in skeletal muscle is a common cause of both sarcopenia and T2DM. Consistently, our study revealed that DEPs are enriched mainly in pathways implicated in lipid metabolism, indicating that lipid metabolism is a critical contributor to the progression of T2DM-related sarcopenia and may be the common root cause of the inter-relationship between T2DM and sarcopenia.

Lipids may exert an impact on cellular activity by altering the composition of cytomembranes, regulating energy reserves, modulating secondary messenger signaling, and influencing gene expression.[30] Fatty acids are common components of various biological lipid species. Normally, skeletal muscle serves as a major site of fatty acid oxidation.[31] The role of fatty acid oxidation in skeletal muscle IR and T2DM is controversial. Some studies have suggested that fatty acid oxidation is decreased in diabetic skeletal muscle. The accumulation of lipids in diabetic skeletal muscle may be attributed to decreased fatty acid oxidation, increased fatty acid uptake, or a combination of both, ultimately causing the skeletal muscle IR and T2DM.[25] However, metabolic competition between fatty acid oxidation and glucose oxidation, termed the "Randle cycle", is well-known to exist in skeletal muscle.[32] Fatty acid oxidation is inhibited, while glucose oxidation is enhanced. Conversely, glucose oxidation is inhibited, while fatty acid levels are enhanced. Consistent with the "Randle cycle", GSEA of the proteomics data set in our study demonstrated that fatty acid oxidation-related pathways were significantly upregulated in T2DM-related sarcopenia mice. Our proteomics analysis suggested that increased fatty acid oxidation may inhibit glucose oxidation and further trigger IR in diabetic skeletal muscle. Although increased fatty acid oxidation may promote the clearance of fatty acids, we found that CD36, a fatty acid transporter responsible for the uptake of fatty acids,[33] is also dramatically upregulated in the skeletal muscle of db/db mice. This finding led us to speculate that fatty acid uptake may exceed fatty acid oxidation, causing the accumulation of fatty acids. Further experimental evidence is needed to test this hypothesis. In addition, it has been reported that tricarboxylic acid cycle (TCA) activity fails to increase with increased fatty acid oxidation, resulting in incomplete fatty acid oxidation and the accumulation of fatty acid intermediates.[32] Moreover, increased fatty acid oxidation is accompanied by oxidative stress, thereby leading to the impairment of insulin signaling and subsequent reductions in muscle mass.[29] A recent study also showed that excessive fatty acid oxidation caused muscle atrophy by oxidative stress in cancer-induced cachexia.[34] Taken together, increased fatty acid oxidation in lipid metabolism plays a critical role in the onset of IR and sarcopenia through direct impacts on glucose oxidation as well as the lipotoxic effects of myosteatosis and oxidative stress.

Fatty acid oxidation includes various processes, including mitochondrial β-oxidation of saturated fatty acids, peroxisomal β-oxidation of very long-chain fatty acids, α-oxidation of branched-chain fatty acids, ω-oxidation, and ketone formation.[30] Among these processes, mitochondrial β-oxidation and peroxisomal β-oxidation are the major fatty acid oxidation pathways.[30] We then constructed a PPI network of the DEPs and identified six hub proteins, namely, ACOX1, CPT2, ECI2, ACADVL, ACADL, and ECH1. Consistent with the GSEA results, these six hub proteins are involved in fatty acid β-oxidation. ACOX1 and ECI2 are the key enzymes involved in peroxisomal β-oxidation, while CPT2, ACADVL, ACADL, and ECH1 participate in mitochondrial β-oxidation. Recently, proteomics research in the skeletal muscle of diabetic and nondiabetic patients also revealed an increased abundance of enzymes, such as ECH1, implicated in fatty acid oxidation in the skeletal muscle of diabetic patients.[35] We also validated the expression of six hub proteins in the GM of db/m and db/db mice by Western blotting and immunohistochemistry. We further conducted a correlation analysis to reveal the significant negative relationships among the six hub proteins and muscle mass and grip strength. Bioinformatics analysis and validation of the hub proteins demonstrated that the key enzymes involved in fatty acid oxidation may be promising targets for the treatment of T2DM-related sarcopenia. Moreover, we further predicted the upstream regulatory mechanism of the hub proteins, which may provide deeper insight into the molecular mechanism of T2DM-related sarcopenia.

The present study has several limitations. First, the proteomics data were derived from a mouse model of T2DM-related sarcopenia. Although our study confirmed that the db/db mouse model is a well-accepted model of T2DM and that sarcopenia is a complication of T2DM, there are still differences between the mouse model and human disease. Further collection of skeletal muscles from patients with T2DM-related sarcopenia is necessary to verify the proteomics data. Second, given that proteins are the predominant executors of biological processes within the cell, we conducted proteomics analysis on skeletal muscle from a mouse model of T2DM-related sarcopenia. Further multiomics studies combining proteomics, transcriptomics, and metabolomics may provide deeper insights into the pathogenesis of

https://doi.org/10.1021/acsomega.4c04668
ACS Omega 2024, 9, 34056−34069

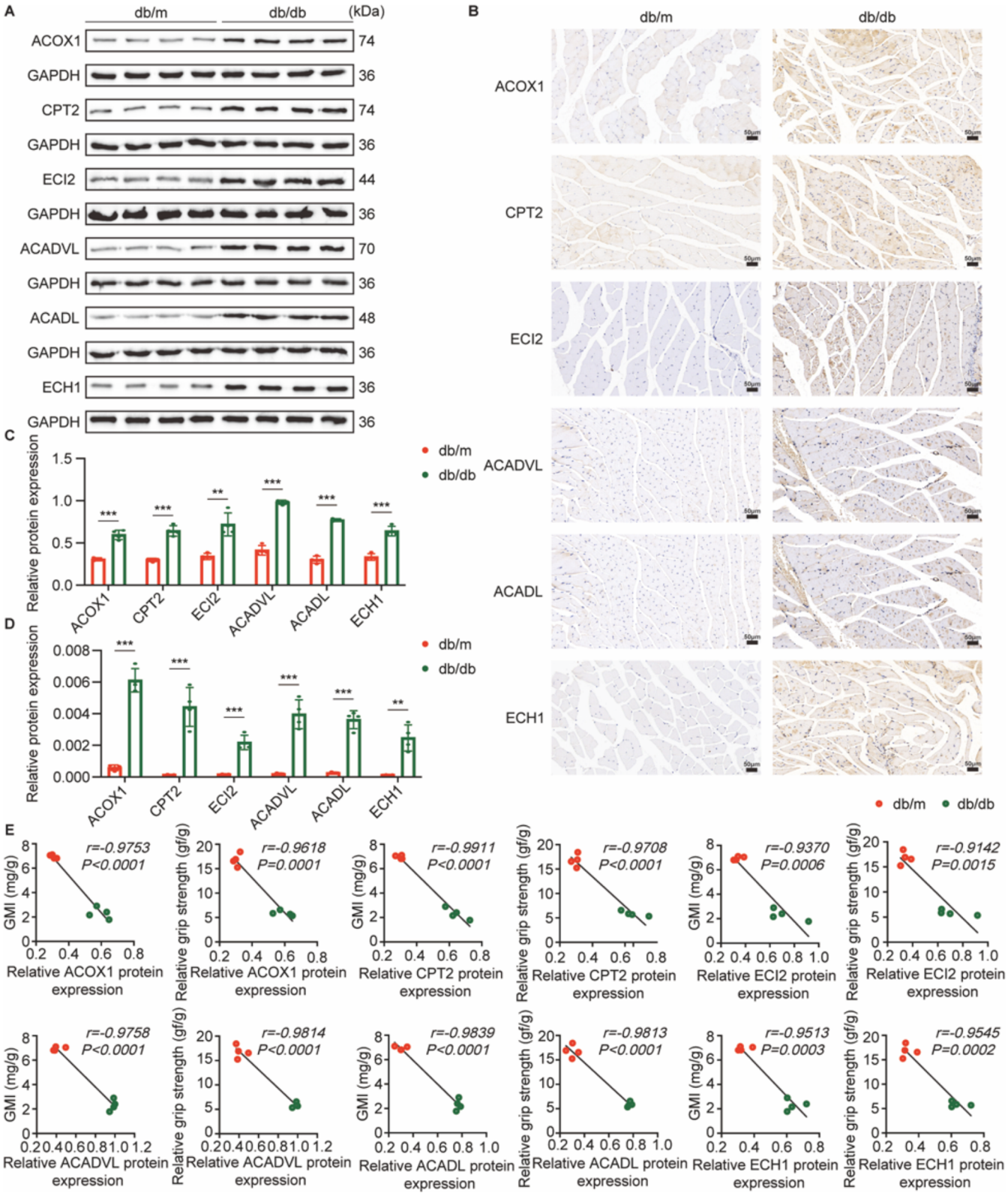

Figure 7. Validation of six candidate hub proteins. (A) Immunoblots of ACOX1, CPT2, ECI2, ACADVL, ACADL, and ECH1 in the GM of db/m and db/db mice. (B) Immunohistochemical staining of ACOX1, CPT2, ECI2, ACADVL, ACADL, and ECH1 in the GM of db/m and db/db mice. Scale bar: 50 μm. (C) Relative expression levels of ACOX1, CPT2, ECI2, ACADVL, ACADL, and ECH1 normalized to GAPDH based on densitometric analysis of immunoblots. (D) Quantitation of immunohistochemical analyses for ACOX1, CPT2, ECI2, ACADVL, ACADL, and ECH1. (E) Correlation analysis of the relative expression levels of ACOX1, CPT2, ECI2, ACADVL, ACADL, and ECH1 with relative grip strength and GMI in mice. Data are expressed as mean ± SD $^{**}P < 0.01$, $^{***}P < 0.001$. $n = 4$ mice per group.

https://doi.org/10.1021/acsomega.4c04668
ACS Omega 2024, 9, 34056−34069

sarcopenia in patients with T2DM. Third, we verified the expression of hub proteins associated with fatty acid oxidation in T2DM-related sarcopenia via Western blotting and immunohistochemistry, while the detailed molecular mechanisms by which these proteins regulate the development of T2DM-related sarcopenia remain unexplored. We are continuing our efforts to carry out further studies on these issues.

CONCLUSIONS

In summary, we investigated the potential mechanisms of T2DM-related sarcopenia using db/db mice, a well-established mouse model of T2DM, through proteomics analysis. Our proteomics data suggest that lipid metabolic disorder may be a fundamental mechanism leading to the progression of T2DM-related sarcopenia and a common cause of the interrelationship between T2DM and sarcopenia. Our work offers valuable insights into the pathogenesis of promising therapeutic targets for treating T2DM-related sarcopenia.

ASSOCIATED CONTENT

Data Availability Statement

The mass spectrometry proteomics data have been deposited to the ProteomeXchange Consortium (https://proteomecentral.proteomexchange.org) via the PRIDE[36] partner repository with the data set identifier PXD051462.

Supporting Information

The Supporting Information is available free of charge at https://pubs.acs.org/doi/10.1021/acsomega.4c04668.

The quality control of mass spectrometry data (Figure S1), functional classification analysis of DEPs (Figure S2), the top 10 KEGG pathways analysis of DEPs (Table S1), the top 5 KEGG pathways analysis of upregulated DEPs (Table S2), and the top 5 KEGG pathways analysis of downregulated DEPs (Table S3) (PDF)

AUTHOR INFORMATION

Corresponding Authors

Chunnuan Chen − *Department of Neurology, Second Affiliated Hospital of Fujian Medical University, Quanzhou, Fujian Province 362000, China*; Email: chenchunnuan1983@aliyun.com

Xiaofeng Chen − *Department of Cardiology, Second Affiliated Hospital of Fujian Medical University, Quanzhou, Fujian Province 362000, China*; orcid.org/0000-0002-2548-8175; Email: 1986xiaofeng0012@163.com

Authors

Jingying Wu − *Department of Cardiology, Second Affiliated Hospital of Fujian Medical University, Quanzhou, Fujian Province 362000, China*

Shengnan Wang − *Department of Cardiology, Second Affiliated Hospital of Fujian Medical University, Quanzhou, Fujian Province 362000, China*

Huafeng Zhuang − *Department of Orthopedics, Second Affiliated Hospital of Fujian Medical University, Quanzhou, Fujian Province 362000, China*

Weichun Wang − *Department of Cardiology, Second Affiliated Hospital of Fujian Medical University, Quanzhou, Fujian Province 362000, China*

Yaoguo Wang − *Department of Cardiology, Second Affiliated Hospital of Fujian Medical University, Quanzhou, Fujian Province 362000, China*

Youfang Chen − *Medical Research Center, Quanzhou Medical College, Quanzhou, Fujian Province 362000, China; Department of Clinical Medicine, Quanzhou Medical College, Quanzhou, Fujian Province 362000, China*

Zhengping Huang − *Department of Neurology, Second Affiliated Hospital of Fujian Medical University, Quanzhou, Fujian Province 362000, China*

Complete contact information is available at: https://pubs.acs.org/10.1021/acsomega.4c04668

Author Contributions

J.Y.W., C.N.C., and X.F.C. conceived and designed research; J.Y.W., H.F.Z., Z.P.H., and C.N.C. collected data and conducted research; J.Y.W., S.N.W., W.C.W., and Y.G.W. analyzed and interpreted data; J.Y.W. and Y.F.C. wrote the initial paper; and C.N.C. and X.F.C. revised the paper. All authors read and approved the final manuscript.

Notes

The authors declare no competing financial interest.

ACKNOWLEDGMENTS

This work was supported by the following funding: the Natural Science Foundation of Fujian Province (2020J01224, 2022J01779), the Quanzhou Science and Technology Program (2023N055S, 2023N057S), and the Second Affiliated Hospital of Fujian Medical University Doctoral Nursery Project (BS202324). The authors appreciate the valuable comments from reviewers.

ABBREVIATIONS

T2DM, type 2 diabetes mellitus; GM, gastrocnemius muscles; GMI, gastrocnemius muscle index; CSA, cross-sectional area; LC-MS/MS, liquid chromatography tandem mass spectrometry; COG/KOG, cluster of orthologous groups/eukaryotic orthologous groups; GO, gene ontology; BP, biological process; CC, cellular component; MF, molecular function; KEGG, Kyoto Encyclopedia of Genes and Genomes; DEPs, differentially expressed proteins; PPI, protein−protein interaction; GSEA, gene set enrichment analysis; HE, Hematoxylin and eosin; ACOX1, acyl-coenzyme A oxidase 1; CPT2, carnitine O-palmitoyltransferase 2; ECI2, enoyl-CoA delta isomerase 2; ACADVL, very long-chain specific acyl-CoA dehydrogenase; ACADL, long-chain specific acyl-CoA dehydrogenase; ECH1, delta (3,5)-delta (2,4)-dienoyl-CoA isomerase; TF, transcription factor; IR, insulin resistance; ROS, reactive oxygen species; FFAs, free fatty acids

REFERENCES

(1) Cruz-Jentoft, A. J.; Sayer, A. A. Sarcopenia. *Lancet* **2019**, *393*, 2636−2646.

(2) Zhang, X.; Zhao, Y.; Chen, S.; Shao, H. Anti-diabetic drugs and sarcopenia: emerging links, mechanistic insights, and clinical implications. *J. Cachexia Sarcopenia Muscle* **2021**, *12*, 1368−1379.

(3) Yan, S.; Liang, H.; Zhan, P.; Zheng, H.; Zhao, Q.; Zheng, Z. Stimulator of interferon genes promotes diabetic sarcopenia by targeting peroxisome proliferator activated receptors γ degradation and inhibiting fatty acid oxidation. *J. Cachexia, Sarcopenia Muscle* **2023**, *14* (6), 2623−2641.

(4) Marcotte-Chénard, A.; Oliveira, B.; Little, J. P.; Candow, D. G. Sarcopenia and type 2 diabetes: Pathophysiology and potential

therapeutic lifestyle interventions. *Diabetes Metab. Syndrome: Clinical Res. Rev.* **2023**, *17*, No. 102835.
(5) DeFronzo, R. A.; Ferrannini, E.; Groop, L.; Henry, R. R.; Herman, W. H.; Holst, J. J.; et al. Type 2 diabetes mellitus. *Nat. Rev. Dis. Primers* **2015**, *1*, No. 15019.
(6) Yang, S.; Yang, G.; Wu, H.; Kang, L.; Xiang, J.; Zheng, P.; et al. MicroRNA-193b impairs muscle growth in mouse models of type 2 diabetes by targeting the PDK1/Akt signaling pathway. *Diabetologia* **2022**, *65*, 563−581.
(7) Sarodnik, C.; Bours, S. P. G.; Schaper, N. C.; Van Den Bergh, J. P.; Van Geel, TACM. The risks of sarcopenia, falls and fractures in patients with type 2 diabetes mellitus. *Maturitas* **2018**, *109*, 70−77.
(8) Trierweiler, H.; Kisielewicz, G.; Hoffmann Jonasson, T.; Rasmussen Petterle, R.; Aguiar Moreira, C.; Zeghbi Cochenski Borba, V. Sarcopenia: a chronic complication of type 2 diabetes mellitus. *Diabetol. Metab. Syndr.* **2018**, *10*, 25.
(9) Feng, L.; Gao, Q.; Hu, K.; Wu, M.; Wang, Z.; Chen, F.; et al. Prevalence and Risk Factors of Sarcopenia in Patients with Diabetes: A Meta-analysis. *J. Clin. Endocrinol. Metab.* **2022**, *107*, 1470−1483.
(10) Chen, H.; Huang, X.; Dong, M.; Wen, S.; Zhou, L.; Yuan, X. The Association Between Sarcopenia and Diabetes: From Pathophysiology Mechanism to Therapeutic Strategy. *DMSO* **2023**, *Volume 16*, 1541−1554.
(11) Mesinovic, J.; Zengin, A.; De Courten, B.; Ebeling, P. R.; Scott, D. Sarcopenia and type 2 diabetes mellitus: a bidirectional relationship. *Diabetes Metab. Syndr. Obes.* **2019**, *12*, 1057−1072.
(12) Lima Leite, A.; Gualiume Vaz Madureira Lobo, J.; Barbosa da Silva Pereira, H. A.; Silva Fernandes, M.; Martini, T.; Zucki, F.; et al. Proteomic analysis of gastrocnemius muscle in rats with streptozotocin-induced diabetes and chronically exposed to fluoride. *PLoS One* **2014**, *9*, No. e106646.
(13) Yu, J.; Loh, K.; Yang, H.-Q.; Du, M.-R.; Wu, Y.-X.; Liao, Z.-Y.; et al. The Whole-transcriptome Landscape of Diabetes-related Sarcopenia Reveals the Specific Function of Novel lncRNA Gm20743. *Commun. Biol.* **2022**, *5*, 774.
(14) Öhman, T.; Teppo, J.; Datta, N.; Mäkinen, S.; Varjosalo, M.; Koistinen, H. A. Skeletal muscle proteomes reveal downregulation of mitochondrial proteins in transition from prediabetes into type 2 diabetes. *iScience* **2021**, *24*, No. 102712.
(15) Savikj, M.; Stocks, B.; Sato, S.; Caidahl, K.; Krook, A.; Deshmukh, A. S.; et al. Exercise timing influences multi-tissue metabolome and skeletal muscle proteome profiles in type 2 diabetic patients - A randomized crossover trial. *Metabolism* **2022**, *135*, No. 155268.
(16) Shi, Z.; Huo, Y.; Hou, J.; Zhang, R.; Wu, J.; Wang, W.; et al. Proteomic analysis of skeletal muscle in Chinese hamsters with type 2 diabetes mellitus reveals that OPLAH downregulation affects insulin resistance and impaired glucose uptake. *Free Radical Biol. Med.* **2022**, *193*, 23−33.
(17) Wang, B.; CC, P.; Pippin, J. J. Leptin- and Leptin Receptor-Deficient Rodent Models: Relevance for Human Type 2 Diabetes. *Curr. Diabetes Rev.* **2014**, *10*, 131−145.
(18) Ferreira, G. S.; Veening-Griffioen, D. H.; Boon, W. P. C.; Hooijmans, C. R.; Moors, E. H. M.; Schellekens, H.; van Meer, P. J. Comparison of drug efficacy in two animal models of type 2 diabetes: A systematic review and meta-analysis. *Eur. J. Pharmacol.* **2020**, *879*, No. 173153.
(19) Mesinovic, J.; Fyfe, J. J.; Talevski, J.; Wheeler, M. J.; Leung, G. K. W.; George, E. S.; et al. Type 2 Diabetes Mellitus and Sarcopenia as Comorbid Chronic Diseases in Older Adults: Established and Emerging Treatments and Therapies. *Diabetes Metab. J.* **2023**, *47*, 719.
(20) Chen, L.-K. The vicious cycle in the development of diabetes mellitus and sarcopenia in older persons. *Arch. Gerontol. Geriatr.* **2021**, *95*, No. 104437.
(21) Veronese, N.; Pizzol, D.; Demurtas, J.; Soysal, P.; Smith, L.; et al. Association between sarcopenia and diabetes: a systematic review and meta-analysis of observational studies. *Eur. Geriatr Med.* **2019**, *10*, 685−696. on behalf of the Special Interest Groups of Systematic Reviews and Meta-Analysis for Healthy Ageing, Diabetes, Sarcopenia of European Geriatric Medicine Society (EuGMS)
(22) Yu, M.; Pan, M.; Liang, Y.; Li, X.; Li, J.; Luo, L. A nomogram for screening sarcopenia in Chinese type 2 diabetes mellitus patients. *Experiment. Gerontol.* **2023**, *172*, No. 112069.
(23) Moriggi, M.; Belloli, S.; Barbacini, P.; Murtaj, V.; Torretta, E.; Chaabane, L.; et al. Skeletal Muscle Proteomic Profile Revealed Gender-Related Metabolic Responses in a Diet-Induced Obesity Animal Model. *IJMS* **2021**, *22*, 4680.
(24) Al Saedi, A.; Debruin, D. A.; Hayes, A.; Hamrick, M. Lipid metabolism in sarcopenia. *Bone* **2022**, *164*, No. 116539.
(25) Gilbert, M. Role of skeletal muscle lipids in the pathogenesis of insulin resistance of obesity and type 2 diabetes. *J. Diabetes Investig* **2021**, *12*, 1934−1941.
(26) Jimenez-Gutierrez, G. E.; Martínez-Gómez, L. E.; Martínez-Armenta, C.; Pineda, C.; Martínez-Nava, G. A.; Lopez-Reyes, A. Molecular Mechanisms of Inflammation in Sarcopenia: Diagnosis and Therapeutic Update. *Cells* **2022**, *11*, 2359.
(27) Kalinkovich, A.; Livshits, G. Sarcopenic obesity or obese sarcopenia: A cross talk between age-associated adipose tissue and skeletal muscle inflammation as a main mechanism of the pathogenesis. *Ageing Res. Rev.* **2017**, *35*, 200−221.
(28) Axelrod, C. L.; Fealy, C. E.; Erickson, M. L.; Davuluri, G.; Fujioka, H.; Dantas, W. S.; et al. Lipids activate skeletal muscle mitochondrial fission and quality control networks to induce insulin resistance in humans. *Metabolism* **2021**, *121*, No. 154803.
(29) Rachek, L. I. Free fatty acids and skeletal muscle insulin resistance. *Prog. Mol. Biol. Transl Sci.* **2014**, *121*, 267−292.
(30) Liu, B.; Meng, Q.; Gao, X.; Sun, H.; Xu, Z.; Wang, Y.; Zhou, H. Lipid and glucose metabolism in senescence. *Front. Nutr.* **2023**, *10*, No. 1157352.
(31) Rasmussen, B. B.; Wolfe, R. R. REGULATION OF FATTY ACID OXIDATION IN SKELETAL MUSCLE. *Annu. Rev. Nutr* **1999**, *19*, 463−484.
(32) Zhang, L.; Keung, W.; Samokhvalov, V.; Wang, W.; Lopaschuk, G. D. Role of fatty acid uptake and fatty acid beta-oxidation in mediating insulin resistance in heart and skeletal muscle. *Biochim. Biophys. Acta* **2010**, *1801*, 1−22.
(33) Li, Y.; Huang, X.; Yang, G.; Xu, K.; Yin, Y.; Brecchia, G.; Yin, J. CD36 favours fat sensing and transport to govern lipid metabolism. *Prog. Lipid Res.* **2022**, *88*, No. 101193.
(34) Fukawa, T.; Yan-Jiang, B. C.; Min-Wen, J. C.; Jun-Hao, E. T.; Huang, D.; Qian, C.-N.; et al. Excessive fatty acid oxidation induces muscle atrophy in cancer cachexia. *Nat. Med.* **2016**, *22*, 666−671.
(35) Fiorentino, T. V.; Monroy, A.; Kamath, S.; Sotero, R.; Cas, M. D.; Daniele, G.; et al. Pioglitazone corrects dysregulation of skeletal muscle mitochondrial proteins involved in ATP synthesis in type 2 diabetes. *Metabolism* **2021**, *114*, No. 154416.
(36) Perez-Riverol, Y.; Bai, J.; Bandla, C.; García-Seisdedos, D.; Hewapathirana, S.; Kamatchinathan, S.; et al. The PRIDE database resources in 2022: a hub for mass spectrometry-based proteomics evidence. *Nucleic Acids Res.* **2022**, *50*, D543−D552.

https://doi.org/10.1021/acsomega.4c04668
ACS Omega 2024, 9, 34056−34069